# PCCP



## **PAPER**



Cite this: Phys. Chem. Chem. Phys., 2022, 24, 11713

# Probing halogen bonding interactions between heptafluoro-2-iodopropane and three azabenzenes with Raman spectroscopy and density functional theory†

Ethan C. Lambert, Da Ashley E. Williams, Dab Ryan C. Fortenberry Da and Nathan I. Hammer 1 \*\*

The potential formation of halogen bonded complexes between a donor, heptafluoro-2-iodopropane (HFP), and the three acceptor heterocyclic azines (azabenzenes: pyridine, pyrimidine, and pyridazine) is investigated herein through normal mode analysis via Raman spectroscopy, density functional theory, and natural electron configuration analysis. Theoretical Raman spectra of the halogen bonded complexes are in good agreement with experimental data providing insight into the Raman spectra of these complexes. The exhibited shifts in vibrational frequency of as high as 8 cm<sup>-1</sup> for each complex demonstrate, in conjunction with NEC analysis, significant evidence of charge transfer from the halogen bond acceptor to donor. Here, an interesting charge flow mechanism is proposed involving the donated nitrogen lone pair electrons pushing the dissociated fluorine atoms back to their respective atoms. This mechanism provides further insight into the formation and fundamental nature of halogen bonding and its effects on neighboring atoms. The present findings provide novel and deeper characterization of halogen bonding with applications in supramolecular and organometallic chemistry.

Received 27th January 2022. Accepted 22nd April 2022

DOI: 10.1039/d2cp00463a

rsc.li/pccp

## Introduction

At the molecular level, noncovalent interactions help guide biological functionality and molecular self-assembly. Among these weak interactions, halogen bonding is of note due to its potential applications in areas such as supramolecular regioselective synthesis, crystal engineering, and drug design. 1-3 Halogen bonds are long distance, noncovalent interactions with strengths comparable to that of hydrogen bonds.<sup>4</sup> A halogen bond forms from an attractive interaction between an electrophilic region, denoted a σ-hole, on a larger halogen atom (typically iodine) and a nucleophilic region on either another molecule of the same or a specimen of a differing molecular system.<sup>5,6</sup> This is contradictory in nature as molecular halides are typically associated with a partial negative

The halogen bond donor chosen for this study is heptafluoro-2-iodopropane (HFP, see Fig. 1), a halogen rich molecule with uses in organometallic synthesis.<sup>8-15</sup> The electron withdrawing fluorinated carbon atoms adjacent to the donor atom, iodine in this case, strengthen its  $\sigma$ -hole which potentially results in stronger halogen bond formation. This molecule is analysed spectroscopically in solution and with computational chemistry when interacting with three potential halogen bond acceptors: pyridine, pyrimidine, and pyridazine.

charge; however, the halogen bond can be better explained in terms of electrostatic potential rather than partial charges. Clark et al.5 provide an extensive review of the formation of the  $\sigma$ -hole and its role in halogen bond formation. In short, when bonds are formed, electronic charge concentrates in bands surrounding the hemisphere of the large halogen atom, creating the  $\sigma$ -hole. This  $\sigma$ -hole is then free to form halogen bonds with nucleophilic regions. Halogen bonds are highly directional, with bond angles varyingly close to 180°, and are denoted in the same manner as hydrogen bonds, R-X···Y, where R represents the donor molecular system, X the halogen itself, and Y the nucleophilic acceptor site. This present work seeks to elucidate halogen bond formation in building block molecules of molecular self-assembly through vibrational spectroscopy in the hopes of aiding future prediction and synthesis of these complexes in supramolecular chemistry.

 $<sup>^</sup>a$  Department of Chemistry and Biochemistry, University of Mississippi, University, Mississippi 38655, USA. E-mail: nhammer@olemiss.edu

<sup>&</sup>lt;sup>b</sup> University of Mississippi Medical Center, School of Medicine, Office of Student Affairs, 2500 N. State Street, Jackson, MS, 39216, USA

<sup>†</sup> Electronic supplementary information (ESI) available: Cartesian coordinates of optimized structures of halogen bonded complexes and the individual molecules, simulated Raman spectra of the halogen bonded complexes at all levels of theory, comparison of simulated Raman spectra of each molecule in isolation and in the complex, comparison of experimental Raman spectra of each molecule in isolation and in the complex. See DOI: https://doi.org/10.1039/d2cp00463a

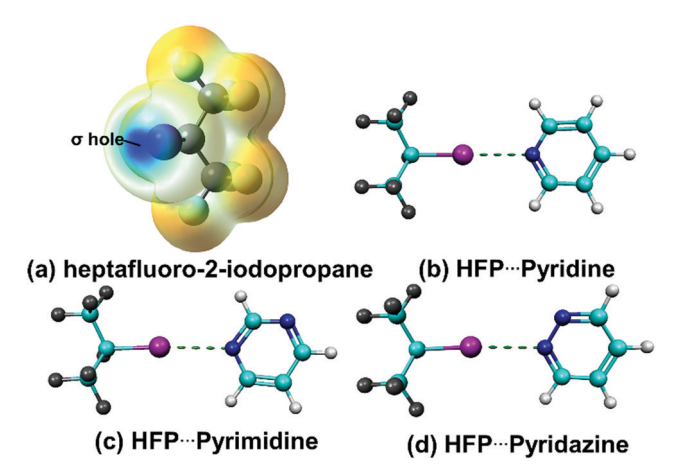


Fig. 1 (a) Electrostatic potential map of heptafluoro-2-iodopropane. The  $\sigma$ -hole region on the iodine atom is indicated. (b–d) Optimized geometry of the halogen bonded complexes at the M06-2X/aVTZ level of theory.

These heterocyclic azines all possess lone pair electrons bound to their one or more nitrogen atoms which could serve as halogen bond acceptors. Nitrogen-containing heterocycles have received much attention in the past as participants in covalent and noncovalent charge transfer interactions. 16-33 Additionally, these studies highlight the usefulness of vibrational spectroscopy, particularly Raman spectroscopy, as a probe of noncovalent interactions. Azines and their derivatives have also been studied in halogen-bonded complexes in the past. 31,34-41 Fan et al. studied HFP in solution with pyridine through coherent anti-Stokes Raman scattering ( $I^{(2)}$ CARS) and conclude that strong halogen bond formation is present. They note that further study of this complex is warranted with a more fundamental vibrational spectroscopic method. Hawthorne et al. further studied HFP with pyridine for potential halogen bond formation with FTIR.<sup>37</sup> Their results show shifts to higher energy in pyridine's ring breathing mode upon halogen bond formation, which is consistent with a past study that correlates shifts to higher energy with charge transfer.<sup>42</sup> To our knowledge, these molecular complexes have not been studied through pure Raman spectroscopy. Further studying of heterocyclic azines with HFP will elucidate charge transfer and the formation of these building block complexes, contributing paramount knowledge to the field of supramolecular and organometallic chemistry.

Along with experimental work, density functional theory (DFT) computations<sup>43</sup> can supplement experimental data. By comparing simulated Raman spectra of the ideal halogen bonded complexes to the experimental data, the structure of the complexes can be deducted. Natural electron configuration (NEC) analysis<sup>44</sup> on these theoretical complexes can also provide further evidence of charge transfer between the species participating in the halogen bond.

This present work employs both DFT and Raman spectroscopy to analyse the formation of HFP halogen bonded complexes with three azabenzenes. Raman spectra of each azabenzene in liquid phase and in solution with HFP are

analysed for shifts in vibrational frequency and compared to simulated Raman spectra to form theoretical models of the experimental results. NEC analysis is utilized to quantify charge transfer upon complex formation. This work will allow for a potentially stronger correlation between shifts in vibrational frequency and charge transfer in molecular complexes to be made. Greater knowledge of halogen bond formation in these complexes will contribute to the prediction and organization of these molecules in organometallic and supramolecular chemistry.

## Methods

98% Heptafluoro-2-iodopropane, 99.8% pyridine, 98.0% pyrimidine, and 99.0% pyridazine were commercially acquired via Sigma-Aldrich and used without further purification. Samples were analysed at room temperature by a Horiba LabRAM HR Evolution Raman Spectroscopy system (Horiba Scientific, Kyoto, Japan) equipped with a 600 grooves per mm grating and charge-coupled device (CCD) detector. A 532 nm Nd:YAG laser (Oxxius, Lannion, France) was used to excite the solutions held in 1 cm glass cuvettes. Spectra were acquired of both individual samples and the three heterocyclic azines separately mixed in equal mole fraction solutions with heptafluoro-2iodopropane. The combination of HFP with any of the azabenzenes can result in an exothermic reaction, causing the formation of an unknown white vapor and the loss of HFP's purple colour. For this reason, experimental measurements were kept at a minimum and caution is advised to those wishing to further study these complexes.

The Becke 3-parameter Lee-Yang-Parr (B3LYP), 44 Minnesota 06-2X (M06-2X),  $^{45}$  and  $\omega$ B97X-D $^{46}$  DFT methods, all with a triple-zeta correlation consistent basis set augmented with diffuse functions (aug-cc-pVTZ, aVTZ),47 are employed for geometry optimizations and computation of the harmonic vibrational frequencies. An additional basis set containing a small-core energy-consistent relativistic pseudopotential (augcc-pVTZ-PP, aVTZ-PP) is necessary for the iodine atoms. 46 This basis set scheme will simply be referred to as aVTZ for the remainder of this work. This follows a similar procedure performed by Ellington et al. 38 Geometry optimizations were performed on each complex in both a planar and antiplanar configuration. Planar refers to a parallel orientation between the carbon chain of HFP and the ring structure of the given heterocyclic azine (see Fig. 1); antiplanar refers to a perpendicular orientation between the two. For frequency computations, a pruned numerical integration grid composed of 99 radial shells and 590 angular points per shell was employed, and harmonic frequencies were scaled by a precomputed vibrational scaling factor of 0.985 to partially account for anharmonicity. 48 Natural bond orbital analyses 49 were also performed on the optimized structures to quantify the magnitude charge transfer  $|\Delta q|$  between the halogen bonded complexes. To map electrostatic potential and total electron density on all molecules, a self-consistent field (SCF) density map was **PCCP Paper** 

employed<sup>50</sup> using a total electron density isosurface value of 0.004 electrons Bohr<sup>-3</sup>, based upon work performed by Ellington et al.38 These computations were performed with the Gaussian 16 software package.<sup>51</sup> Cartesian coordinates of the optimized complexes and HFP are available in the ESI.†

When comparing specific modes in experimental and theoretical spectra, graphs are normalized to highlight specific modes, resulting in changes in peak ratio. Full experimental and theoretical spectra for all molecules and complexes are available in the ESI.†

## Results and discussion

#### Structural effects

The electrostatic potential (ESP) was mapped using a SCF density calculation to show evidence of a  $\sigma$ -hole in HFP. Fig. 1a shows the area of positive electrostatic potential on the proximal surface of the iodine atom. The  $\sigma$ -hole has an ESP of 0.097 a.u.; this is almost double that of the belt of lower ESP on the outer edge of the atom, having an ESP of 0.054 a.u. This agrees with past studies34,37 of HFP and shows its potential for halogen bond donation.

Molecular energies for each optimized planar and antiplanar structure show the planar configuration to be, on average, 0.01 kcal mol<sup>-1</sup> lower in energy than the antiplanar for each DFT method. For all complexes, the M06-2X/aVTZ method and basis set showed no imaginary vibrational frequencies, providing evidence of a local minimum structure for the planar conformer. The optimized planar geometries are shown in Fig. 1b-d. The M06-2X/aVTZ computations are used for comparison throughout the remainder of this study. See ESI,† Fig. S1-S3 for all theoretical methods compared to experimental results.

Table 1 provides the C-I bond lengths (r(C-I) Å), halogen bond distances (r(XB) Å), and halogen bond dissociation enthalpies (XB Diss. E (kcal mol<sup>-1</sup>)) for all three halogen bonded complexes in addition to the C-I bond length for the halogen bond donor. Upon formation of the halogen bonded complex, each C-I bond lengthens due to the attractive interaction between the  $\sigma$ -hole and the nitrogen lone pairs causing delocalization in the C-I bond. The greatest lengthening of the C-I bond is observed in the pyridine containing complex (0.018 Å), shortly followed by the approximately equal lengthening of the pyrimidine and pyridazine complexes (0.013 Å). Halogen bond distances follow an inverse trend of the lengthening of the C-I bond, with a longer C-I bond correlating to a

**Table 1** Changes in C-I bond lengths (r(C-I) Å), halogen bond distances (r(XB) Å), and halogen bond dissociation enthalpies (XB Diss. E (kcal mol<sup>-1</sup>)) for all three halogen bonded complexes and the halogen bond donor

Molecule	<i>r</i> (C−I) Å	<i>r</i> (XB) Å	XB Diss. $E$ (kcal mol <sup>-1</sup> )
HFP	2.142	X	X
HFP···Pyridine	2.160	2.841	6.971
HFP···Pyrimidine	2.155	2.905	7.010
HFP···Pyridazine	2.156	2.879	8.464

shorter halogen bond distance. Halogen bond dissociation enthalpies were calculated at 298.15 K and 1.000 atm; the greatest dissociation enthalpy is in the pyridazine complex (8.464 kcal mol<sup>-1</sup>), decreasing with the pyrimidine complex (7.010 kcal mol<sup>-1</sup>) and decreasing even more with the pyridine complex  $(6.971 \text{ kcal mol}^{-1})$ .

#### Spectroscopic results

Table 2 contains the experimental and theoretical frequencies for the three C-I stretching motions as well as the ring breathing mode of the complexes and isolated molecules. To distinguish between these stretching motions, an ESI† figure depicts the displacement vectors of the vibrations. This table will be referenced throughout the remainder of this study. Fig. 2 shows the simulated Raman spectra compared to experimental data for the HFP···Pyridine, HFP···Pyrimidine, and HFP···Pyridazine halogen bonded complexes. The simulated spectra agree with experimental data concerning the number of Raman active modes for all three complexes. However, the computed vibrational energies in the fingerprint region are shifted higher in energy than what is observed experimentally, even after accounting for anharmonicity. This phenomenon is best portrayed in the pyridazine complex with the ring breathing mode predicted to be almost 80 cm<sup>-1</sup> higher in energy than experiment. The C-H stretching region (approximately 3000 cm<sup>-1</sup>) is also predicted to occur higher in energy for all complexes with several mode splittings. As computations are performed in an isolated environment, intermolecular interactions such as pistacking, self-halogen bonding, and electrostatic repulsion in condensed phases, believed to be the cause of the lower vibrational energies seen in experimental data, are not incorporated in the computations.

To highlight the bellwether vibrations of halogen bond formation, Raman spectra focusing on the harmonic frequencies involving the C-I stretch modes (3) and the ring breathing mode (1) in the halogen bonded complexes are compared to those of the individual molecules in Fig. 3. The first C-I stretch of all three complexes is shifted lower in energy relative to that of isolated HFP: 7 cm<sup>-1</sup> in the pyridine and pyridazine complexes and 4 cm<sup>-1</sup> in the pyrimidine complex. For each halogen bonded structure, a shift to higher energy of the ring breathing mode relative to the isolated azabenzenes is also present: 8 cm<sup>-1</sup> in pyridine, 7 cm<sup>-1</sup> in pyrimidine, and 3 cm<sup>-1</sup> in pyridazine. Interestingly, the ring breathing mode in the pyrimidine complex does not fully form a new peak higher in energy unlike the other two heterocyclic azines. As pyrimidine has two halogen bond acceptor sites, the equal mole fraction of HFP was not sufficient to completely saturate all sites, leaving some pyrimidine molecules without complex formation. Hypothetically, a 0.66 mole fraction solution of HFP should efficiently saturate pyrimidine with halogen bonds (2 molecules of HFP for each pyrimidine molecule).

The second and third frequencies including contribution from the C-I stretch show no trend between complexes as the first C-I stretch frequencies do. Normal mode analysis shows the first C-I involves a simultaneous movement of the iodine

Table 2 Frequencies (cm<sup>-1</sup>) of the three C-I stretching motions and the ring breathing mode

	Experiment				Theory			
Molecule	1st C-I stretch	2nd C-I stretch	3rd C–I stretch	Ring breathe	1st C-I stretch	2nd C-I stretch	3rd C–I stretch	Ring breathe
Neat Pyridine/HFP	254	749	899	993	264	759	921	977
HFP···Pyridine	247	751	902	1001	254	758	925	1016
Shift	-7	2	3	8	-10	-1	4	39
Neat Pyrimidine/HFF	254	749	899	991	264	759	921	957
HFP···Pyrimidine	250	751	903	998	257	758	926	1017
Shift	-4	2	4	7	-7	-1	5	60
Neat Pyridazine/HFP	254	749	899	962	264	759	921	948
HFP···Pyridazine	247	748	900	965	256	758	940	1039
Shift	-7	-1	1	3	-8	-1	19	91

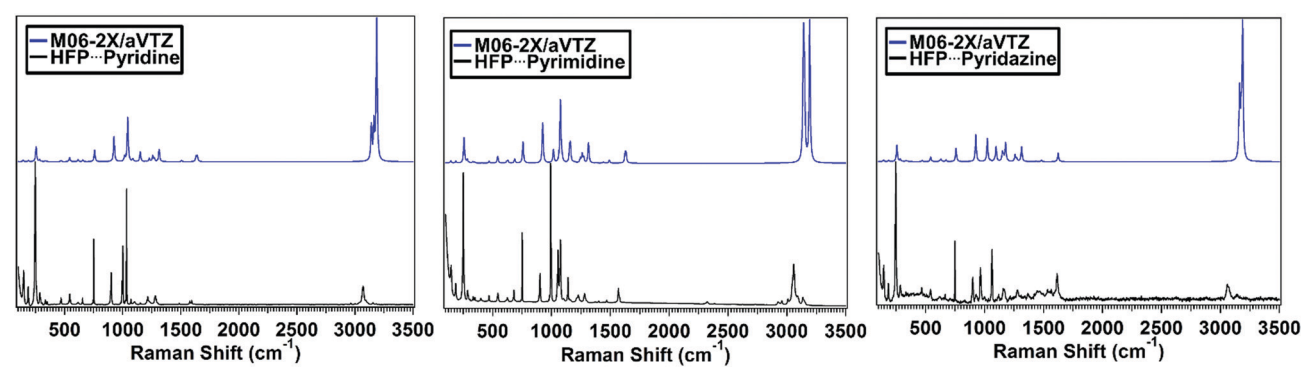


Fig. 2 Simulated and experimental Raman spectra for the halogen bonded complexes.

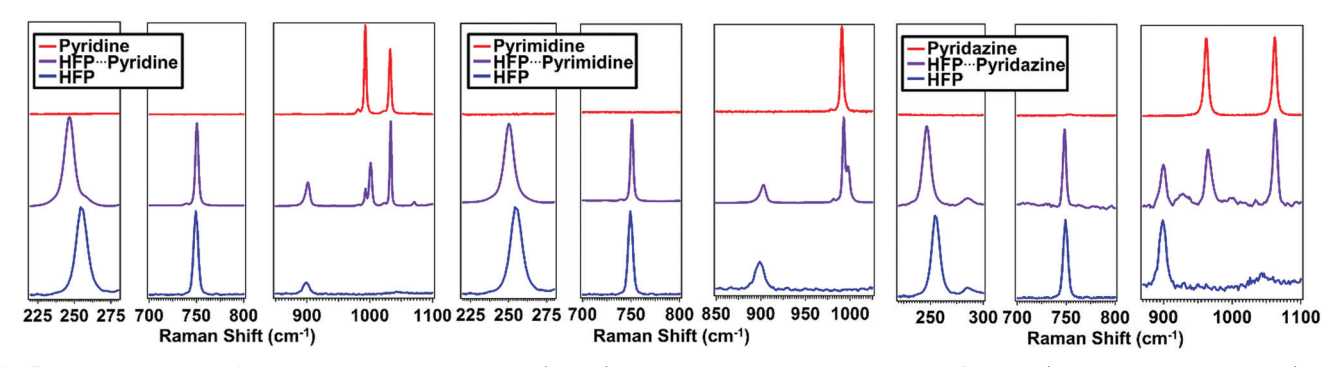


Fig. 3 Raman spectrum of the halogen bonded complexes (purple) compared to the individual molecules' spectra (azabenzene, red; HFP blue).

atom and its alpha carbon, *i.e.* both the alpha carbon and the iodine atom are symmetrically drawn to a central location in the bond length. This stretching motion is shifted to lower frequency as charge is received in the complex formation. In the second and third C–I stretches, the iodine atom is largely fixed in place, resulting in little influence on these vibrational frequencies due to the complex formation.

To compare these harmonic frequencies to those predicted in theory, simulated Raman spectra of the C-I stretches and ring breathing modes in the halogen bonded complexes and individual molecules are demonstrated in Fig. 4. In the pyridine and pyrimidine complexes, DFT accurately recovers all shifts in the observed vibrational modes. In the pyridazine complex,

however, theory accurately predicts the shift to lower energy of the first frequency involving the C–I stretch, while also predicting large shifts to higher energy for the remaining C–I stretches and the ring breathing mode that do not occur experimentally. This disagreement in the shifting of pyridazine's vibrational modes alludes to some interaction within the solution phases reducing the perturbation of pyridazine's electronic structure.

A broader look at the data of all three halogen-bonded complexes yields the appearance of a series of trends between the structural, vibrational, and electronic properties of the halogen bonded complexes. Shorter perturbations of the C–I bond correspond to smaller, higher-frequency shifts of the first C–I stretching motion in both experiment and in theory. This

**PCCP Paper** 

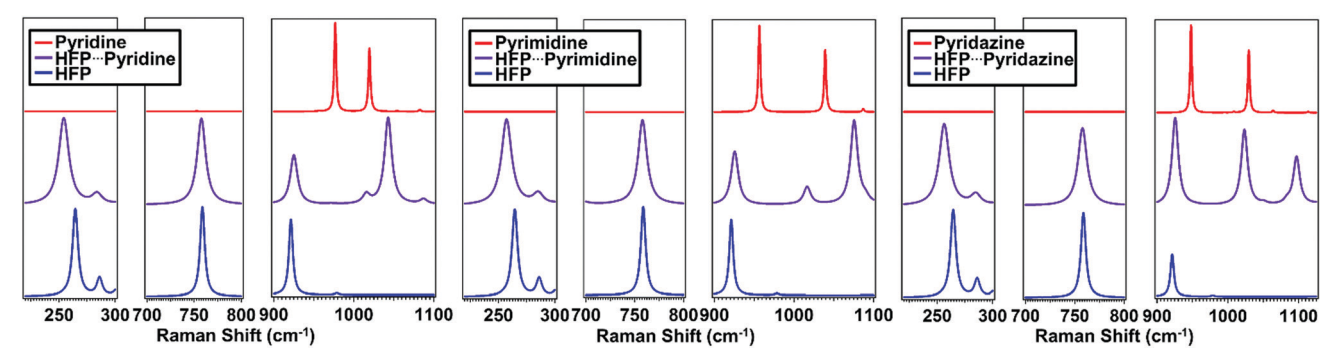


Fig. 4 Simulated Raman spectrum of the halogen bonded complexes (purple) compared to the individual molecules' spectra (azabenzene, red; HFP blue) at the M06-2X/aVTZ level of theory.

trend is also seen with decreased halogen bond distance. With more delocalized, stronger halogen bonds, the electronic the experimental shift in the ring breathing mode of each complex, presumably for these same reasons.

#### Quantifying the flow of charge

As previously discussed in the introduction and results, shifts in vibrational spectra are indicative of perturbation in the underlying electronic structure. Charge transfer is common between molecules in noncovalently-bound complexes and is believed to be the driving force behind the shifts seen here. To quantify this charge transfer, differences in Natural Electron Configurations (NEC) were calculated for each molecule and complex; these results are listed in the ESI.† The Raman spectra above imply halogen bond formation, presumably from a

withdrawal of electron density structure undergoes a greater disturbance, leading to a larger shift in vibrational frequency. Longer halogen bonds also reduce from nitrogen's lone pair to the  $\sigma$ -hole on iodine. Counterintuitively, the natural population of the iodine is shown to decrease, and the accepting nitrogen atom's natural population increases in the complexes relative to that in the isolated molecules. Charge transfer from nitrogen to iodine is hypothesized here to be present in the complexes; however, the transfer of nitrogen's lone pair electrons into the antibonding C-I molecular orbital pushes the fluorine lone pair electrons back to their respective atoms. This is supported by the increase in natural population of the fluorine atoms closer to the halogen bond and by the alpha carbon atoms mediating the charge transfer to the skeleton of HFP. The depletion of the accepting nitrogen atom's charge causes it to pull electron

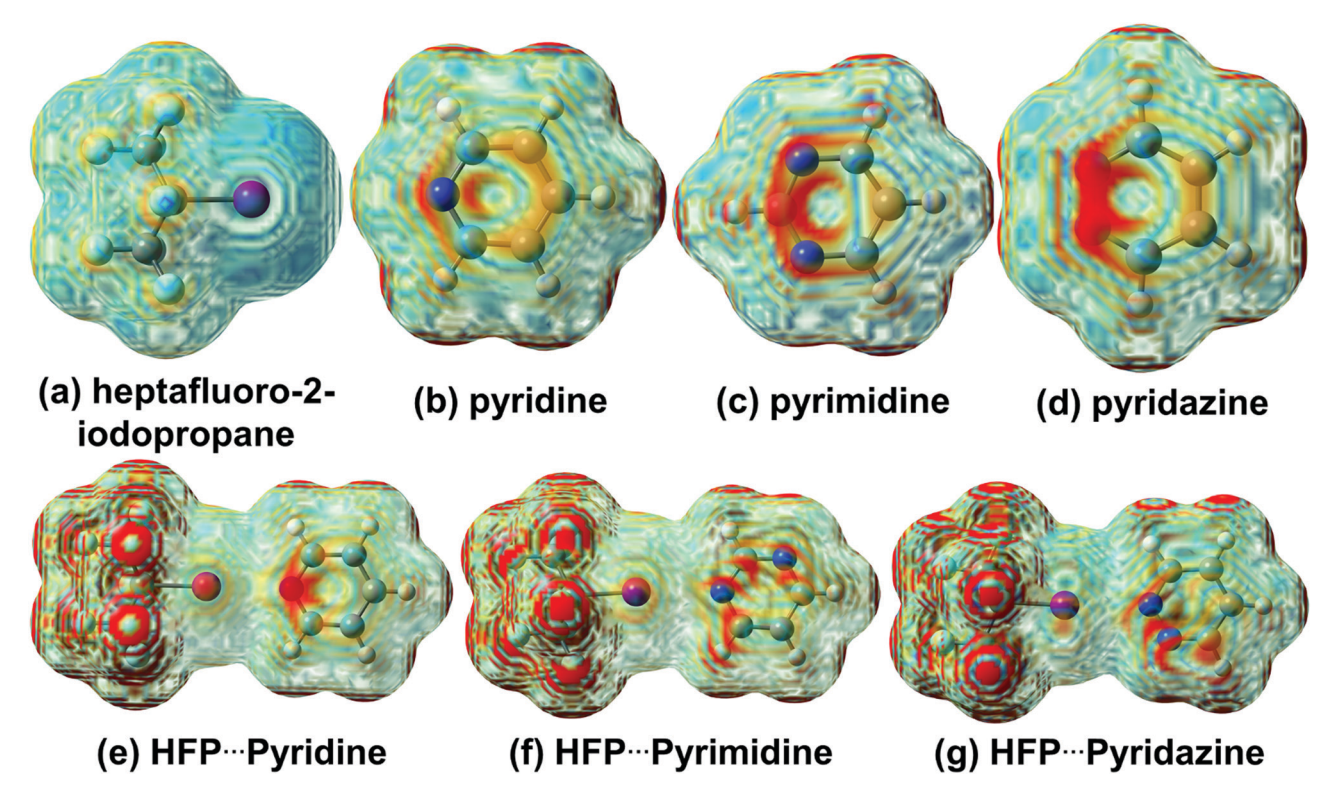


Fig. 5 Total electron density plots of all neat molecules and halogen bonded complexes.

**Table 3** E(2) delocalization energies for the halogen bonded complexes

	E(2) Delocalization energy				
Molecule	$\frac{\text{LP(N)} \rightarrow \sigma^*(\text{C-I})}{\text{kcal mol}^{-1}}$	$LP(F) \rightarrow \sigma^*(C-I)$ kcal mol <sup>-1</sup>			
HFP···Pyridine	11.45	11.48			
HFP· · · Pyrimidine	9.13	12.17			
HFP· · · Pyridazine	9.75	11.59			
Neat HFP	X	11.97			

density from its neighbouring carbon and/or nitrogen atoms. At a fundamental level, this charge transfer correlates with shifts in vibrational frequencies and offers evidence of halogen bond formation in the halogen bonded complexes. To demonstrate this shift in electronic population, Fig. 5 contains total electronic density (TED) plots of all molecules and complexes with increasing electron density transitioning from blue to red. Upon formation of the halogen bond, electronic density shifts towards the fluorine atoms on the halogen bond donor as electronic charge is transferred into the  $\sigma$ -hole of the iodine atom. To counteract this depletion of charge, the nitrogen atom draws electron density from the rest of the ring structure. Interestingly, the structures containing two nitrogens feature a swirling of electronic density shift due to a somewhat cyclic nature of electronic charge withdrawal. These plots agree with the NEC.

In order to add further evidence for this proposed mechanism, E(2) delocalization energies  $^{49,52}$  for the halogen bonded complexes are presented in Table 3. Of the systems analysed here, the strongest delocalization of the nitrogen lone pair is with the HFP···Pyridine complex (11.45 kcal mol $^{-1}$ ), followed by the pyridazine and pyrimidine complexes, (9.75 and 9.13 kcal mol $^{-1}$  respectively). Interestingly, with increasing LP(N)  $\rightarrow \sigma^*(\text{C-I})$  delocalization energy comes decreasing LP(F)  $\rightarrow \sigma^*(\text{C-I})$  delocalization energy. The delocalization of the nitrogen lone pair electrons into the antibonding orbital of the C-I bond appears to push the fluorine lone pair electrons

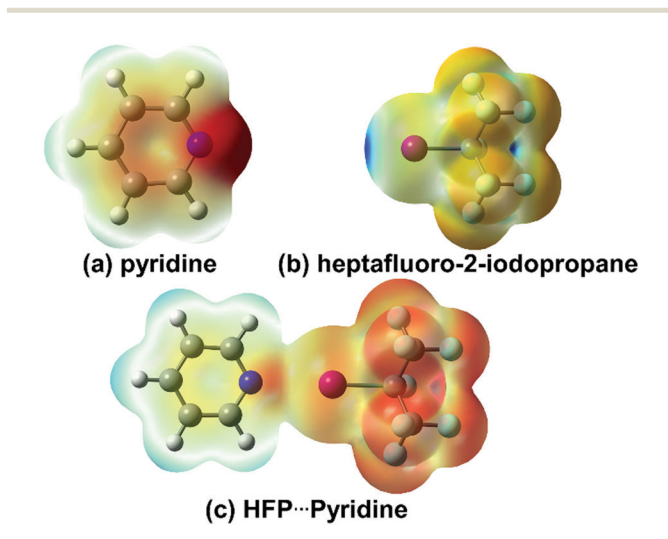


**Fig. 6** Electrostatic potential maps of (a) pyridine, (b) heptafluoro-2-iodopropane (HFP), and (c) the HFP···Pyridine complex.

back towards their respective atoms. This is supported by the inverse relation between the LP(N)  $\rightarrow$   $\sigma^*(C-I)$  and LP(F)  $\rightarrow$  $\sigma^*(C-I)$  delocalization energies. Exemplifying this effect is the pyridine complex having a delocalization energy of 11.48 kcal mol<sup>-1</sup>, followed by pyridazine with 11.59 kcal mol<sup>-1</sup> and pyrimidine with 12.17 kcal mol<sup>-1</sup>. Interestingly, compared to neat HFP, the pyrimidine complex increases total LP(F)  $\rightarrow$  $\sigma^*(C-I)$  delocalization energy whilst still showing increases in TED. This agrees with the inverse relationship seen between  $LP(F) \rightarrow \sigma^*(C-I)$  and  $LP(N) \rightarrow \sigma^*(C-I)$  delocalization energies. The flow of charge in the halogen bonded complexes induces changes in electrostatic potential, illustrated for the pyridine complex in Fig. 6, which directly compares the electrostatic potential for the isolated molecules and the resulting halogenbonded complex. The hydrogen atoms become noticeably more positive (blue-green), while the fluorine atoms become much more negative (red).

The E(2) delocalization energies also provide insight into other trends. The shift in experimental and theoretical first C–I stretching frequencies and ring breathing modes is correlated with decreasing LP(N)  $\rightarrow \sigma^*(C-I)$  delocalization energy and increasing LP(F)  $\rightarrow \sigma^*(C-I)$  delocalization energy. This trend likely arises from the transfer of charge into the antibonding C–I orbital causing perturbations of the electronic structure, leading to the relationship between greater LP(N)  $\rightarrow \sigma^*(C-I)$  delocalization energies and larger shifts in vibrational frequency. Based upon the E(2) delocalization energy of the nitrogen lone pairs, the shifts in experimental and theoretical frequencies, and the halogen bond distances, the HFP···Pyridine complex appears to form the strongest halogen bond, followed, respectively, by the pyridazine and pyrimidine complexes.

## Conclusions

Halogen bond formation in three molecular complexes yields shifts in vibrational spectra and perturbation of electronic populations and E(2) delocalization energies. Evidence is given for the mechanism in charge flow upon complex formation. Raman spectroscopy and DFT computations demonstrate shifts in vibrational frequency of both the halogen bond donor, heptafluoro-2-iodopropane and the three acceptors, pyridine, pyrimidine, and pyridazine. Shifts to lower frequency for the lowest frequency modes involving the C-I stretch and small shifts to higher frequency for the second and third C-I stretches along with the ring breathing modes all relative to the isolated molecules are observed upon their attractive intermolecular interactions in solution. NEC analysis and E(2)delocalization energies reveal a depletion of the iodine atom's natural population. A charge flow mechanism is proposed here where the charge donation causes the fluorine lone pairs to be pushed back into their respective atoms allowing the halogen bond serves as a conduit for electronic charge. This is supported as the fluorine atoms closest in proximity to the halogen bond show increases in natural population and decrease in

**PCCP Paper** 

delocalization energy with the antibonding C-I orbital in all three complexes. The pushing mechanism is also supported by an inversely proportional relationship between LP(N)  $\rightarrow \sigma^*$ (C-I) and LP(F)  $\rightarrow \sigma^*$ (C-I) delocalization energies. This charge flow mechanism should be exhibited in similar systems using fluorine atoms to increase the positive electrostatic potential of the  $\sigma$ -hole. Furthermore, this charge flow mechanism likely dictates the formation of halogen bonds in such systems and has far reaching implications in predicting complex formation, charge transfer events, self-assembly and other manifestations stemming from similar weak intermolecular interactions in fields such as organometallic and supramolecular chemical synthesis.

## **Author contributions**

The manuscript was written through contributions of all authors. All authors have given approval to the final version of the manuscript. Individual author contributions are as follows: Ethan C. Lambert, conceptualization, formal analysis, investigation, visualization, writing - original draft, writing review and editing; Dr Ashley E. Williams, formal analysis, investigation, methodology, validation, writing - review and editing; Dr Ryan C. Fortenberry, methodology, validation, writing - original draft, writing - review and editing; Dr. Nathan I. Hammer, funding acquisition, project administration, resources, software, supervision, writing - original draft, writing - review and editing.

## Conflicts of interest

There are no conflicts to declare.

# Acknowledgements

This work has been supported by the National Science Foundation (OIA-1757220 and CHE-1532079) as well as the Sally McDonnell Barksdale Honors College at the University of Mississippi. The computations in this letter were performed using resources at the Mississippi Center for Supercomputing Resources (MCSR). Thanks to Prof. Jared Delcamp (University of Mississippi) for his advisement in working with these chemicals.

## Notes and references

- 1 P. Metrangolo, F. Meyer, T. Pilati, G. Resnati and G. Terraneo, Angew. Chem., Int. Ed., 2008, 47, 6114-6127.
- 2 P. Metrangolo, H. Neukirch, T. Pilati and G. Resnati, Acc. Chem. Res., 2005, 38, 386-395.
- 3 R. Wilcken, M. O. Zimmermann, A. Lange, A. C. Joerger and F. M. Boeckler, J. Med. Chem., 2013, 56, 1363-1388.
- 4 P. Metrangolo and G. Resnati, Halogen Bonding: Fundamentals and Applications, 2008.

5 T. Clark, M. Hennemann, J. S. Murray and P. Politzer, J. Mol. Model., 2007, 13, 291-296.

- 6 G. R. Desiraju, P. S. Ho, L. Kloo, A. C. Legon, R. Marquardt, P. Metrangolo, P. Politzer, G. Resnati and K. Rissanen, Pure Appl. Chem., 2013, 85, 1711-1713.
- 7 P. Politzer, J. S. Murray and T. Clark, Phys. Chem. Chem. Phys., 2010, 12, 7748-7757.
- 8 R. E. Banks, A. Braithwaite, R. N. Haszeldine and D. R. Taylor, J. Chem. Soc. A, 1969, 996-1000, DOI: 10.1039/j39690000996.
- 9 R. D. Chambers, J. Hutchinson, R. H. Mobbs and W. K. R. Musgrave, Tetrahedron, 1964, 20, 497-506.
- 10 R. D. Chambers, W. K. R. Musgrave and J. Savory, J. Chem. Soc., 1962, 1993-1999, DOI: 10.1039/jr9620001993.
- 11 C. M. De Vöhringer and E. H. Staricco, J. Chem. Soc., Faraday Trans. 1, 1984, 80, 2631-2637.
- 12 R. S. Dickson and G. D. Sutcliffe, Aust. J. Chem., 1972, 25, 761-768.
- 13 G. L. Fleming, R. N. Haszeldine and A. E. Tipping, J. Chem. Soc., Perkin Trans. 1, 1973, 574-577, DOI: 10.1039/ p19730000574.
- 14 H. D. Hartmann, H. Knöckel and E. Tiemann, Chem. Phys. Lett., 1985, 113, 364-367.
- 15 H. Millauer, Angew. Chem., Int. Ed. Engl., 1973, 12, 929.
- 16 G. R. Desiraju and T. Steiner, The Weak Hydrogen Bond in Structural Chemistry and Biology, 1999.
- 17 C. E. Dykstra and J. M. Lisy, J. Mol. Struct.: THEOCHEM, 2000, **500**, 375–390.
- 18 S. J. Grabowski, Hydrogen Bonding New insights, 2006.
- 19 D. Hadzi, Theoretical Treatments of Hydrogen Bonding, 1997.
- 20 W. C. Hamilton and J. A. Ibers, Hydrogen Bonding in Solids, 1968.
- 21 P. Hobza, R. Zahradník and K. Müller-Dethlefs, Collect. Czech. Chem. Commun., 2006, 71, 443-531.
- 22 G. A. Jeffrey, An Introduction to Hydrogen Bonding, 1997.
- 23 G. A. Jeffrey and W. Saenger, Hydrogen Bonding in Biological Structures, 1991.
- 24 K. Müller-Dethlefs and P. Hobza, Chem. Rev., 2000, 100, 143-167.
- 25 L. Pauling, The Nature of the Chemical Bond and the Structure of Molecules and Crystals, 1960.
- 26 G. C. Pimentel and A. L. McClellan, The Hydrogen Bond, 1960.
- 27 S. Scheiner, Molecular Interactions. From van der Waals to Strongly Bound Complexes, 1997.
- 28 S. Scheiner, Hydrogen Bonding: A Theoretical Perspective,
- 29 P. Schuster, G. Zundel and C. Sandorfy, The Hydrogen Bond. Recent Developments in Theory and Experiments, 1976.
- 30 D. A. Smith, Modeling the Hydrogen Bond, 1994.
- 31 A. E. S. Hardin, T. L. Ellington, S. T. Nguyen, A. L. Rheingold, G. S. Tschumper, D. L. Watkins and N. I. Hammer, Inorganics, 2019, 7, 119.
- 32 A. A. Howard, G. S. Tschumper and N. I. Hammer, J. Phys. Chem. A, 2010, 114, 6803-6810.
- 33 E. C. Lambert, B. W. Stratton and N. I. Hammer, ACS Omega, 2022, 7(15), 13189–13195.

34 H. Fan, J. K. Eliason, C. Diane Moliva A, J. L. Olson, S. M. Flancher, M. W. Gealy and D. J. Ulness, *J. Phys. Chem.* A, 2009, 113, 14052–14059.

- 35 V. Stilinović, G. Horvat, T. Hrenar, V. Nemec and D. Cinčić, *Chem. Eur. J.*, 2017, 23, 5244–5257.
- 36 W. X. Wu, H. C. Liu and W. J. Jin, *Chem. Eur. J.*, 2021, 28(2), e202103336.
- 37 B. Hawthorne, H. Fan-Hagenstein, E. Wood, J. Smith and T. Hanks, *Int. J. Spectrosc.*, 2013, 2013, 216518.
- 38 T. L. Ellington, P. L. Reves, B. L. Simms, J. L. Wilson, D. L. Watkins, G. S. Tschumper and N. I. Hammer, *Chem-PhysChem*, 2017, **18**, 1267–1273.
- 39 T. L. Ellington, K. L. Shuford and D. P. Devore, J. Phys. Chem. A, 2020, 124, 10817–10825.
- 40 C. I. Nwachukwu, L. J. Patton, N. P. Bowling and E. Bosch, *Acta Crystallogr., Sect. C: Struct. Chem.*, 2020, **76**, 458–467.
- 41 H. Zhu, J. Wu and G. Dai, J. Mol. Model., 2020, 26, 333.
- 42 A. M. Wright, A. A. Howard, J. C. Howard, G. S. Tschumper and N. I. Hammer, *J. Phys. Chem. A*, 2013, 117, 5435–5446.
- 43 K. Burke and L. O. Wagner, *Int. J. Quantum Chem.*, 2013, 113, 96–101.
- 44 K. Kim and K. D. Jordan, *J. Phys. Chem.*, 1994, 98, 10089–10094.
- 45 Y. Zhao and D. G. Truhlar, *Theor. Chem. Acc.*, 2008, **120**, 215-241.
- 46 J.-D. Chai and M. Head-Gordon, *Phys. Chem. Chem. Phys.*, 2008, **10**, 6615–6620.
- 47 T. H. Dunning, J. Phys. Chem., 1989, 90, 1007-1023.

- 48 I. M. Alecu, J. Zheng, Y. Zhao and D. G. Truhlar, *J. Chem. Theory Comput.*, 2010, **6**, 2872–2887.
- 49 F. Weinhold and C. R. Landis, *Chem. Educ. Res. Pract.*, 2001, 2, 91–104.
- 50 I. G. Csizmadia, in *Computational Advances in Organic Chemistry: Molecular Structure and Reactivity*, ed. C. Ögretir and I. G. Csizmadia, Springer, Netherlands, Dordrecht, 1991, pp. 1–165, DOI: 10.1007/978-94-011-3262-6 1.
- 51 M. J. Frisch, G. W. Trucks, H. B. Schlegel, G. E. Scuseria, M. A. Robb, J. R. Cheeseman, G. Scalmani, V. Barone, G. A. Petersson, H. Nakatsuji, X. Li, M. Caricato, A. V. Marenich, J. Bloino, B. G. Janesko, R. Gomperts, B. Mennucci, H. P. Hratchian, J. V. Ortiz, A. F. Izmaylov, J. L. Sonnenberg, Williams, F. Ding, F. Lipparini, F. Egidi, J. Goings, B. Peng, A. Petrone, T. Henderson, D. Ranasinghe, V. G. Zakrzewski, J. Gao, N. Rega, G. Zheng, W. Liang, M. Hada, M. Ehara, K. Toyota, R. Fukuda, J. Hasegawa, M. Ishida, T. Nakajima, Y. Honda, O. Kitao, H. Nakai, T. Vreven, K. Throssell, J. A. Montgomery Jr., J. E. Peralta, F. Ogliaro, M. J. Bearpark, J. J. Heyd, E. N. Brothers, K. N. Kudin, V. N. Staroverov, T. A. Keith, R. Kobayashi, J. Normand, K. Raghavachari, A. P. Rendell, J. C. Burant, S. S. Iyengar, J. Tomasi, M. Cossi, J. M. Millam, M. Klene, C. Adamo, R. Cammi, J. W. Ochterski, R. L. Martin, K. Morokuma, O. Farkas, J. B. Foresman and D. J. Fox, Gaussian 16, Gaussian, Inc., Wallingford CT, 2016.
- 52 J. Joy, E. D. Jemmis and K. Vidya, *Faraday Discuss.*, 2015, 177, 33–50.